JOURNAL OF SOLID STATE CHEMISTRY **127,** 64–71 (1996)
ARTICLE NO. 0357

Substitution of Chromium for Univalent Copper in Superconducting $Pb_2Sr_2(Ca,Y)Cu_3O_{8+\delta}$

R. Seshadri, A. Maignan, M. Hervieu, C. Martin, and B. Raveau

Laboratoire CRISMAT, CNRS URA 1318, ISMRA et Université de Caen, Bd. du Maréchal Juin, 14050 Caen Cedex, France

and

C. N. R. Rao

Solid State and Structural Chemistry Unit and CSIR Center of Excellence in Chemistry, Indian Institute of Science, Bangalore 560 012 India

Received June 12, 1996; in revised form August 6, 1996; accepted August 8, 1996

Following considerations of geometry and the similarity between chromate and carbonate groups in terms of size and charge, we have investigated the possibility of replacing the two-coordinate Cu^I in superconducting lead cuprates of the general formula $Pb_2Sr_2(Ca, Y)Cu_3O_8$ by Cr. A high-resolution electron microscopy study coupled with energy dispersive X-ray analysis on small crystals of the title phases suggests that between 10 and 15% of the Cu^I can be replaced by Cr. While from the present structural study using HRTEM and Rietveld refinement of X-ray powder data we are unable to precisely obtain the oxidation state and oxygen coordination of Cr, we suggest in analogy with Cr substitution in other similar cuprates that in the title phases Cu^IO_2 rods are partially replaced by tetrahedral CrO_4^{2-} groups. Infrared spectroscopy supports the presence of CrO_4^{2-} groups. The phases $Pb_{1.75}Sr_2Ca_{0.2}Y_{0.8}Cu_3O_{8+\delta}$ and $Pb_{1.75}Sr_2Ca_{0.2}Y_{0.8}Cu_{2.85}Cr_{0.15}O_{8+\delta}$ are superconducting as-prepared, but the substitution of Cr for Cu^I results in a decrease of the T_C as well as the superconducting volume fraction.

INTRODUCTION

The superconducting lead cuprates of the general formula $Pb_2Sr_2(Ca, Y)Cu_3O_{8+\delta}$, first prepared by Cava *et al.* (1) can be described as ordered intergrowths along **c** between a Pb_2CuO_2 block with an anion-deficient K_2NiF_4 ''0201'' structure and a $(Y, Ca)Sr_2Cu_2O_6$ block with an anion-deficient $Sr_3Ti_2O_7$ ''0212'' structure. The stacking sequence along **c** is –(Cu)(PbO)(SrO)(CuO_2)(Y)(CuO_2)(SrO)(PbO)–. If we recast the structure of Y $Ba_2Cu_3O_{7-\delta}$, more commonly ''123,'' in a similar fashion, we obtain the stacking sequence –(CuO)(BaO)(CuO_2)(Y)(CuO_2)(BaO)– making evident the similarity between the two structures. A closer examination of these two structures reveals the presence in both of a low-valent Cu atom, sandwiched between $[PbO]_\infty$ layers with two nearest oxygens in the ''0201–0212'' structure, and sandwiched between $[BaO]_\infty$ layers with four nearest oxygens in the ''123'' structure. One might therefore expect the substitution chemistry at this low-valent Cu site in the two structures to be similar.

The substitution of the triangular CO_3^{2-} group for low-valent Cu in the CuO chain-site of the ''123'' structure has been known for some time (2). Thus phases such as $(Y, Ca)Sr_2(Cu,C)_3O_{7-\delta}$ can be prepared and rendered superconducting under high oxygen pressure (3). Using image simulation of high-resolution electron micrographs, the copper oxycarbonate $Y_4Sr_8Cu_{11}(CO_3)O_{25}$ has been shown as having every fourth CuO_4 square replaced by a triangular CO_3 (4). In a similar manner GaO_4 tetrahedra are known to replace CuO_4 squares in the phase $YSr_2GaCu_2O_7$ (5). An examination of the CO_3^{2-} group in the K_2NiF_4-related copper oxycarbonate $Sr_2Cu(CO_3)O_2$ (S_2CC) (6) shows that the distance between two of the three oxygen atoms coordinated with copper and forming a chain along **c** in the structure is about 2.7 Å. This is on the order of the distance between oxygen atoms in CrO_4^{2-} tetrahedra in $\alpha - K_2CrO_4$ (7). Considering that CO_3^{2-} and CrO_4^{2-} have the same charge, it might be expected that their chemistries be comparable. In Fig. 1, we have sketched these two oxyanions in a manner that emphasizes the similarity. In the lower half of this figure, we have tried to indicate the similarity of coordination of the low-valent Cu in the ''123'' and ''0201–0212'' structures. We see from this figure that for the CO_3^{2-} or CrO_4^{2-} oxyanions to substitute Cu, a strain

0022-4596/96 $18.00

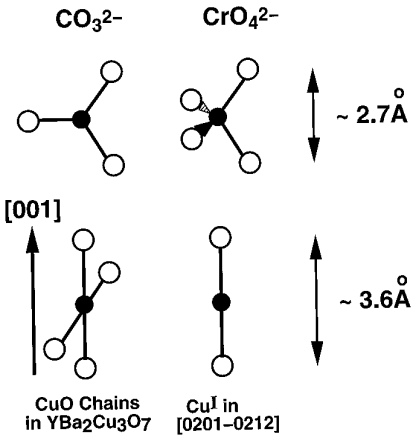

FIG. 1. Schematic representations of the CO_3^{2-} and the CrO_4^{2-} oxyanions, and the coordination of low-valent Cu in the ''123'' and ''0201–0212'' structures. The importance O–O distances are also shown.

of about 25% must be overcome. Such substitution must therefore involve some rearrangement of neighboring metal–oxygen planes. We note that Cr substitution for Cu in the chain site of ''123'' has been reported (8, 9), the phases becoming superconducting after treatment under high oxygen pressures. However, the nature of the CrO_n polyhedra in these systems has not, to our knowledge, been determined.

Likewise, the Hg, Tl, or Pb ions in the rock salt layers of mercury, thallium, or lead high T_C cuprates can be partly replaced by transition metals. Superconducting copper oxycarbonates comprising intergrowths of Hg or Tl cuprates with the S_2CC phase are also amenable to such substitution. Often, the substitution takes place with no detriment to the superconducting properties and in certain cases actually serves to ensure the stabilization of the particular phase as well as to improve the properties. The examples include especially, the mercury based superconductors $Hg_{1-x}M_xBa_2Ca_{m-1}Cu_mO_{2m+2+\delta}$ which are easily formed for M = V, Mo, W, Ti, Cr (10, 11). The similar strontium containing mercury cuprates $Hg_{1-x}M_xSr_2Ca_{m-1}Cu_mO_{2m+2+\delta}$ (12, 13) cannot be stabilized under normal pressure without such substitution at the Hg site. In many of the mercury cuprates, the Hg ion is largely two-coordinate, resembling in some sense, Cu^I in the ''0201–0212'' phase. Among the transition metals, chromium exhibits particular behavior. It has been demonstrated in the mercury (14) and thallium (15, 16) cuprates that CrO_4^{2-} groups can replace Hg and Tl polyhedra in an ordered way. Again, in these cases, the structures can be compared with those of certain oxycarbonates (17), with CrO_4^{2-} tetrahedra replacing the CO_3^- triangles. We mention here that the study of these materials by high-resolution electron microscopy is facilitated by the fact that these small oxyanionic groups appear as very bright spots in lattice images.

As an outcome of the considerations presented in the preceding discussion, we have attempted to substitute Cr for Cu^I in the superconducting Pb-based cuprates of the ''0201–0212'' family, following structure, by powder X-ray diffraction and electron microscopy, as well as superconducting properties. We were indeed able to replace some of the Cu^I by Cr in these phases, but at some detriment to the superconducting properties. We present the results

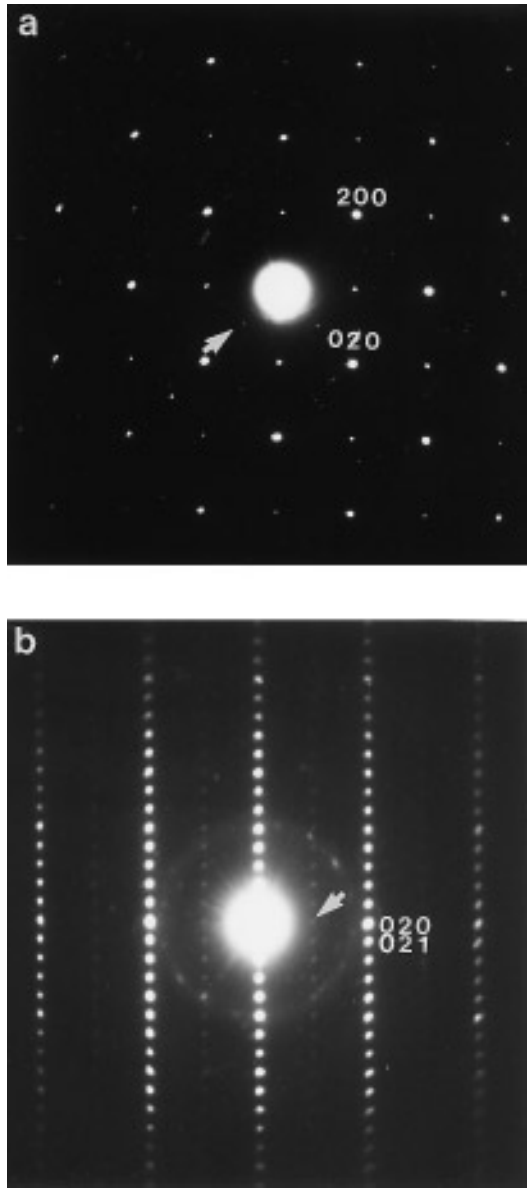

FIG. 2. (a) [001] and (b) [100] electron diffraction patterns. Weak reflections showing that the *c*-type symmetry is violated are indicated by white arrows.

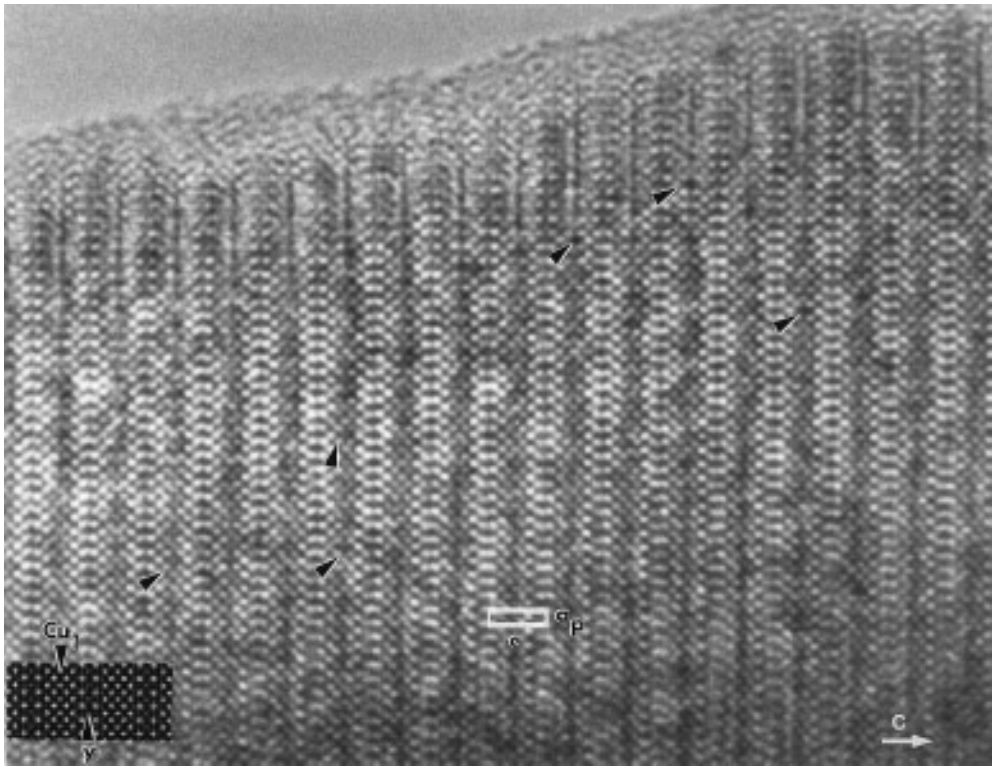

FIG. 3. [110] HREM image. The periodiciy along [001] and [110] is outlined (d_{110} is labeled a_P). The calculated image of the ideal "0201–0212" structure is superposed in the left part of the experimental image ($\Delta f \sim 550$ Å and crystal thickness ~30 Å). Some of the point defects are indicated by black triangles.

here as evidence for the rich substitutional chemistry possible in these systems.

EXPERIMENTAL

Keeping in mind the rather critical nature of doping in these systems, phases were prepared, initially, according to the formulation

- $Pb_2Sr_2Ca_{1-y}Y_yCu_{3-x}Cr_xO_{8+\delta}$.

The syntheses were carried out in two steps. First suitable proportions of $SrCO_3$, $CaCO_3$, Y_2O_3, and CuO were ground intimately and fired in dense alumina crucibles between 1173 and 1273 K for about 48 hr with intermediate grinding. These precursors were then ground together with suitable amounts of PbO and Cr_2O_3, placed in dense alumina crucibles, sealed in silica tubes under a vacuum of 10^{-2} Torr, and fired at 1173 K for 10 hr. After the firing, the tubes were quenched to ambient temperatures. The addition of Cr_2O_3 in the first step did not result in clean phases. This preparative strategy resulted in superconducting phases without the necessity for post-annealing. Phases were made with different Ca/Y ratios, for $y = 0.5, 0.8, 1$. Lead deficiency was also introduced after it was found that it resulted in purer phases.

The formation of the phase was ascertained using a Guinier–deWolff X-ray camera. Powder X-ray diffraction patterns were recorded in the Bragg–Brentano geometry on a Philips PW3710 based vertical diffractometer using Cu$K\alpha$ radiation in the 2θ range of 4°–100°, using a step-scan interval of 0.02°. The XND program was used for the Rietveld refinement of the X-ray data (18). Transmission electron microscopy coupled with energy dispersive X-ray (EDS) analysis was performed on a JEOL 200CX electron microscope fitted with a tilting/rotating sample holder and on a TOPCON 002B microscope, having a point resolution of 1.8 Å. The images were simulated using the MacTempas program. Fourier transform infrared (FTIR) spectra were acquired in the transmission geometry in pressed KBr pellets on a Nicolet Magna 750 spectrometer. The superconducting properties were followed using a Quantum Design SQUID magnetometer in a 10 G field. Demagnetization corrections were not applied.

RESULTS

Phase Formation and Electron Microscopy

From the Guinier X-ray films, it was clear that the "0201–0212" cuprates could be synthesized by following

the above process. The formation of Cr-doped phases was found possible only for relatively small Ca : Y ratios. Analysis of the X-ray diffraction patterns suggested that the introduction of Cr in the starting compositions resulted in changes in the lattice parameters and an increase in the orthorhombic strain, $2 \times (a - b)/(a + b)$ as discussed later. The full yttrium composition was impure when prepared under the conditions followed here and the introduction of Cr in the structure in the absence of Ca was not successful.

EDS analyses were systematically performed on the different samples, varying x and y. It clearly confirmed that the maximum Cr content is about 0.15 per formula unit and that the Ca : Y ratio never exceeds 0.25. This will be discussed further.

The electron diffraction study showed that the cell parameters are $a \sim b \sim \sqrt{2}a_P$ and $c = 15.7$ Å, where a_P refers to the ideal perovskite cell. The conditions limiting the reflections hkl, $h + k = 2n$ are in agreement with a $Pb_2Sr_2(Ca,Y)Cu_3O_8$-type phase. However weak reflections are systematically observed that show that the *C*-type symmetry is violated. Two examples are shown in Figs. 2a and 2b. In the [001] ED pattern (Fig. 2a) $0kl$ reflections with $k = 2n + 1$ are observed. These weak reflections are indicated by white arrows. They suggest that the actual symmetry is *P*-type. Such features have been reported in the undoped materials (19, 20), so they can be considered as being intrinsic to the ''0201–0212'' structure.

A high resolution electron microscopy study was carried out on a sample with a nominal composition of $x = 0.25$ and $y = 0.8$. HREM images exhibit contrast which confirms the stacking model along **c** is that expected for the ''0201–0212'' phase. An example of the [110] HREM is given in Fig. 3. Along that direction, which corresponds to the $[100]_P$ direction of the perovskite subcell, the different layers can be easily identified. For this focus value, assumed to be close to −550 Å, the cation positions are highlighted. The two rows of intense dots 3.4 Å apart are correlated to the two CuO_2 layers. The layer sequence (SrO)(PbO)(Cu^I)(PbO)(SrO) appears as five staggered rows of less bright dots. The theoretical image calculated for the positional parameters given in Table 1 is superimposed on the experimental HREM image in Fig. 3. The simulation allows the following observations to be made:

• The layer stacking along **c** is very regular. Very few intergrowths are observed, in contrast to the undoped material where numerous defects have been noted (20).

• A nonuniform contrast is observed at the level of the (PbO)(Cu^I)(PbO) layer in a systematic way. These variations suggest the existence of point defects at the level of the Cu^I layer. It results from the local variation of the dot brightness coupled with displacement of the surrounding atoms. Some of these defects are indicated by small arrows in Fig. 3b. At the level of the (PbO) layer, only weak variations of contrast are observed, correlated to the point defects at the Cu^I layer.

TABLE 1
Results of Rietveld Refinement on the Average Structure

Model with Cr replacing Cu^I
Composition: $Pb_{1.75}Ca_{0.2}Sr_2YCu_{2.85}Cr_{0.15}O_8$
Space group: *Cmmm* (No. 65)
$a = 5.3860(7)$ Å, $b = 5.4195(7)$ Å, $c = 15.720(2)$ Å
$R_{Bragg} = 10.2\%$, $R_F = 9.9\%$, $R_{WP} = 11.4\%$, $R_P = 8.8\%$, GoF = 1.7

Atom	Site	x	y	z	B (Å^2)[a]	Occupancy in formula[b]
Pb	4*l*	0	1/2	0.3870(2)	0.91(8)	1.75
Ca	4*l*	0	1/2	0.3870(2)	0.91(8)	0.20
Sr	4*k*	0	0	0.2208(3)	0.50(15)	2
Y	2*a*	0	0	0	1.49(18)	1
Cu(1)	2*d*	0	0	1/2	1.49(18)	0.85
Cr	2*d*	0	0	1/2	1.49(18)	0.15
Cu(2)	4*l*	0	1/2	0.1084(5)	0.50(15)	2
O1	4*l*	0	1/2	0.2625(22)	1	2
O2	4*k*	0	0	0.3850(20)	1	2
O3	8*m*	1/4	1/4	0.1007(13)	1	4

Bond lengths

Bond			Length	Multiplicity
(Pb, Ca)	4*l*	–O1	1.96(1)	1
		–O2	2.69(1)	2
		–O2	2.71(1)	2
Y	2*a*	–O3	2.48(1)	8
(Cu(1), Cr)	2*d*	–O2	1.81(1)	2
Sr	4*k*	–O1	2.77(1)	2
		–O1	2.79(1)	2
		–O2	2.58(1)	1
		–O3	2.69(1)	4
Cu(2)	4*l*	–O1	2.42(1)	1
		–O3	1.91(1)	4

[a] Refined in blocks according to site symmetry. Not refined for oxygen.
[b] As suggested by the TEM/EDS analysis.

The origin of such defect-like features could be related to the substitution of Cu^I by chromium, accompanied by the insertion of additional oxygen surrounding the Cr ion. The variation of contrast would result from the cummulative effect of atomic displacements rather than solely from the substitution of Cr for Cu, since the scattering factors of Cr and Cu are nearly equal. Support for the presence of extra oxygen around Cr comes from FTIR spectra, shown in Fig. 4, of two samples with the compositions $Pb_{1.75}Ca_{0.2}Sr_2Y_{0.8}Cu_3O_{8+\delta}$ and $Pb_{1.75}Ca_{0.2}Sr_2Y_{0.8}Cu_{2.85}Cr_{0.15}O_{8+\delta}$. In the latter, the presence of peaks corresponding to vibrations of the CrO_4^{2-} tetrahedra around 800 cm^{-1} are clearly visible, apart from a small contribution due to adventitious carbonate present in the phases with and without Cr. In the Cr free phase, these modes are absent.

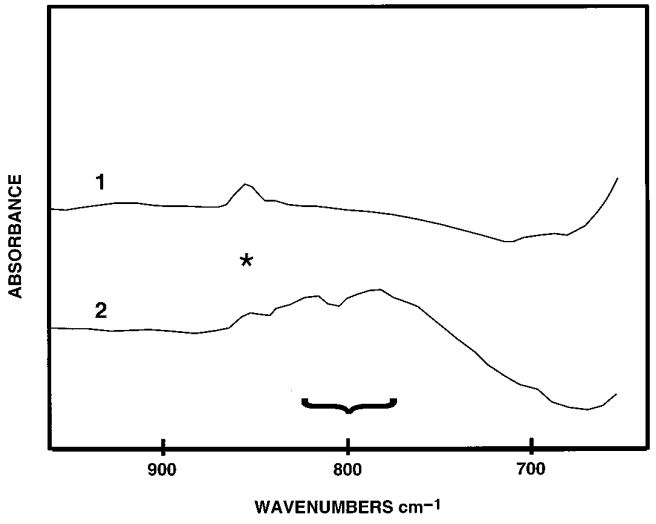

FIG. 4. A portion of the FTIR spectrum of (**1**) $Pb_{1.75}Ca_{0.2}Sr_2Y_{0.8}Cu_3O_{8+\delta}$ and (**2**) $Pb_{1.75}Ca_{0.2}Sr_2Y_{0.8}Cu_{2.85}Cr_{0.15}O_{8+\delta}$. The peaks marked with an asterisk are due to adventitious carbonate. The contribution from CrO_4^{2-} in the region around 800 cm^{-1} is indicated.

Keeping in mind the accuracy limitations of the technique, the EDS analysis indicates a lead and copper deficiency with respect to the content of yttrium and strontium. The average composition seems to be close to $Pb_{1.75}Sr_2Ca_{0.2}YCu_{2.85}Cr_{0.15}$, calculated by fixing the Sr content to 2 per unit. The HREM images suggest that Cr and Cu^I are located in the intermediate layer, so that Ca is expected to occupy the rock-salt layer with Pb. This would allow the structure to be reformulated as $(Pb_{1.75}Ca_{0.2})Sr_2Y(Cu^I_{0.85}Cr_{0.15})Cu_2O_{8+\delta}$.

Rietveld Refinement of $Pb_{1.75}Ca_{0.2}Sr_2YCu_{2.85}Cr_{0.15}O_{8+\delta}$

We show in Fig. 5 the effect of Cr substitution on the lattice parameters in the phases $Pb_{1.75}Ca_{0.2}Sr_2YCu_{3-x}Cr_xO_{8+\delta}$. The x values are notional, corresponding to the starting composition. There is a perceptible increase in the orthorhombic strain on substitution of Cr for Cu, but the behavior of the cell parameters is otherwise complex, testifying to the nature of the substitution comprising more than just simple alloying. Following the suggestion from TEM/EDS that the best phases are formed with high Y content and that Cr does replace Cu^I, we have carefully studied samples with the initial compositions $Pb_{1.75}Sr_2Ca_{0.2}Y_{0.8}Cu_{2.85}Cr_{0.15}O_{8+\delta}$ and $Pb_{1.75}Sr_2Ca_{0.2}YCu_{2.85}Cr_{0.15}O_{8+\delta}$ by Rietveld analysis of powder X-ray data. Figure 6 shows the data and fitted profile of the former phase, along with the difference profile and the simulated contributions from impurities (fitted by pattern-matching). The starting coordinates for the refinement were taken from the work of Cava *et al.* (1) and Kadowacki *et al.* (21). The *Cmmm* space group was used for the refinement even though microscopy results suggest that the actual symmetry is monoclinic. However, the weakness of the extra reflections observed in the electron diffraction study due to the P-type symmetry suggest that a change in the space group would not be significant at the resolution of the X-ray data used for refinement. The occupations were as suggested by the electron microscopy/EDS study and are seen from Fig. 6 to satisfactorily model the experimental pattern. The samples were never absolutely phase pure. Impurities can be seen in the X-ray pattern in Fig. 6, in the 2θ region between 25° and 30°. We were unable to identify the impurities, but suspect as others (20) that they belong to the Ca–Sr–Pb–O phase diagram. The data are tabulated in Table 1. In the description used, the oxygen coordination around the Cr atoms is not described very well because Cr randomly replaces Cu^I and because X-rays are relatively insensitive to oxygen. For a better description of the structure around Cr, a more local probe

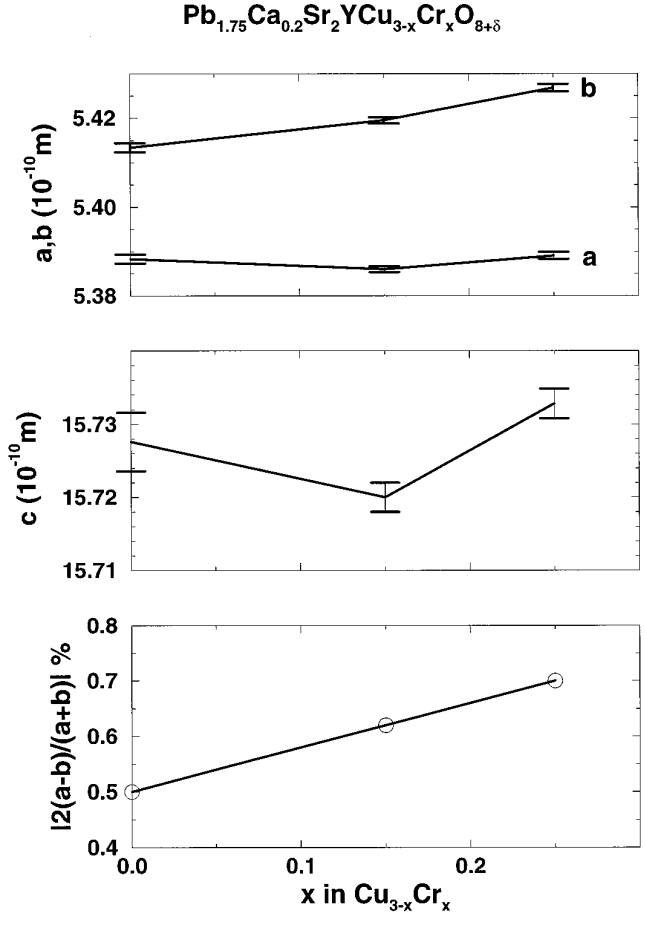

FIG. 5. Lattice parameters and orthorhombic strain in $Pb_{1.75}Ca_{0.2}Sr_2YCu_{3-x}Cr_xO_{8+\delta}$ as a function of the substitution index x. The solubility limit is around $x = 0.15$.

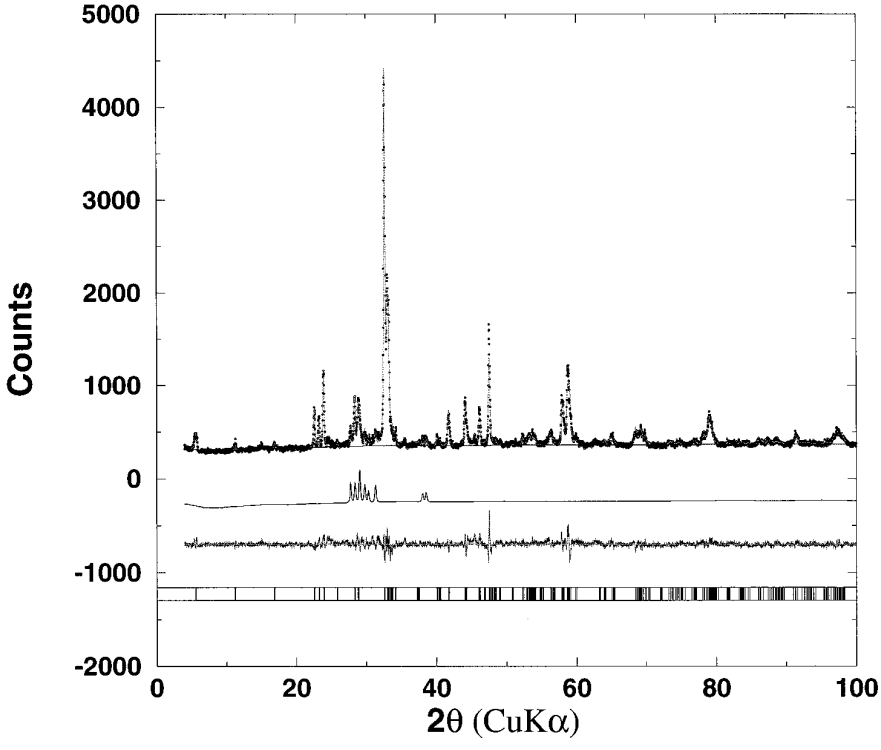

FIG. 6. Powder X-ray diffraction pattern of a sample with the initial composition $Pb_{1.75}Ca_{0.2}Sr_2Ca_{0.2}Y_{0.8}Cu_{2.85}Cr_{0.15}O_{8+\delta}$. The small circles are the data and the line is the profile refined as described in the text. The difference between the data and the fitted profile, and the simulated contribution of impurities are indicated below the experimental spectrum. Vertical lines mark expected reflection positions.

such as X-ray absorption fine structures may be required. However an increase in the orthorhombic strain on Cr substitution and a rather poor description of the 220 reflection at around a 2θ value of $\sim 47°$ due to an inadequately described Cu^I site support the model of Cr substituting this site. Other models for the refinement, for example, smaller occupancies of Y, larger occupancies of Pb, or Cr in the Pb site, resulted in poorer refinements, both in terms of reliability factors and poorly described thermal parameters. Figure 7a shows a schematic structure of the parent "0201–0212" phase in a reduced ($a_P \times a_P \times c$) representation. This is the model used in the refinement. In Fig. 7b, a model for the replacement of the OCu^IO rods by the tetrahedral CrO_4^{2-} group along with some distortions in the PbO layers is shown.

Superconducting Properties

We confine our discussion on superconductivity in these samples to the two systems $Pb_{1.75}Sr_2Ca_{0.2}YCu_{3-x}Cr_xO_{8+\delta}$ and $Pb_{1.75}Sr_2Ca_{0.2}Y_{0.8}Cu_{3-x}O_{8+\delta}$. While HREM (as well as a Rietveld analysis of the occupancy at the Y site) suggests that in most phases the yttrium occupancy is nearly unity, we could, with full yttrium occupancy, obtain phases dis-

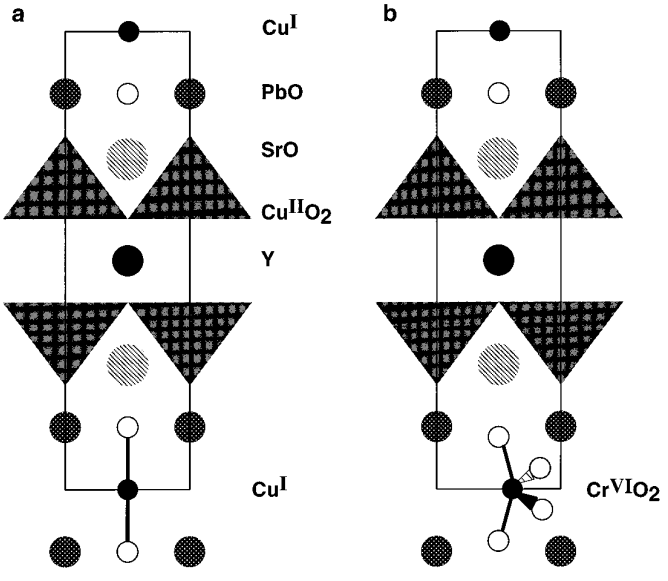

FIG. 7. (a) Structure in a simplified $a_P \times a_P \times c$ representation of the "0201–0212" phase. (b) Suggested coordination around Cr substituted in the Cu^I site.

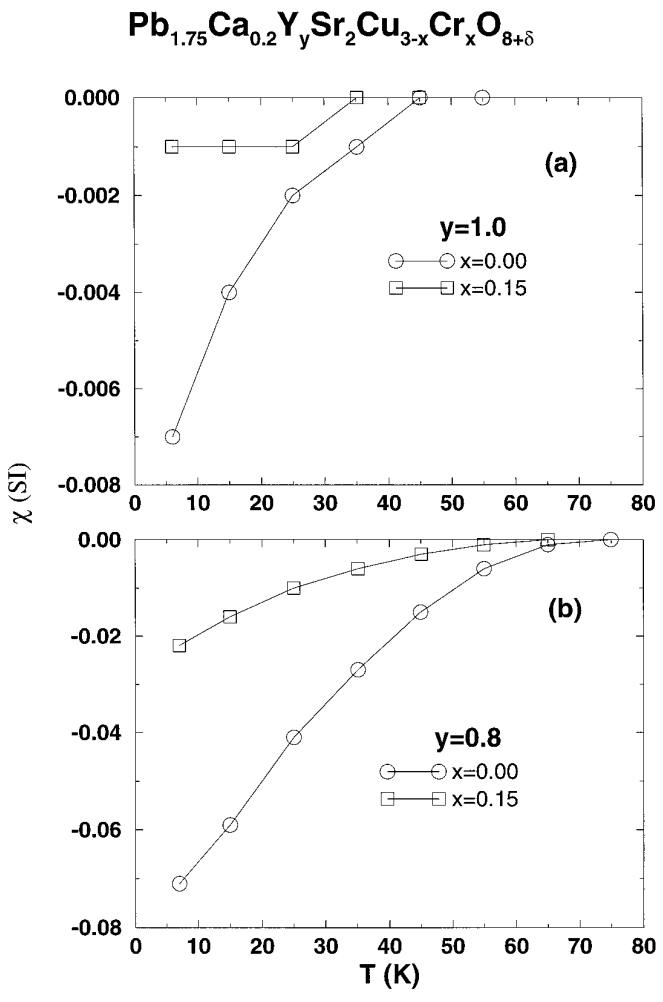

FIG. 8. (a) Volume magnetic susceptibility as a function of temperature of samples (in the form of small, sintered bars) with the initial composition $Pb_{1.75}Ca_{0.2}Sr_2Y_yCu_{2.85}Cr_{0.15}O_{8+\delta}$. The value of x and y are indicated in the figure. (b) The same as in (a) but with a nominal Y deficiency ($y = 0.8$) in the initial composition.

playing only traces of superconductivity. This is seen from the temperature dependence of the volume magnetic susceptibility in Fig. 8a. In this phase, the Ca is nominally considered as occupying the Pb site. In Fig. 8b, the susceptibility of phases with $y = 0.8$ are shown. We see that the Cr-free phase shows a T_C(onset) of 75 K and a total Meissner fraction of about 7% at low temperatures. This value is small, but is characteristic of polycrystalline samples in the ''0201–0212'' system. Nominal substitution of 15% Cr in the Cu^I site resulted in both T_C as well as the Meissner fraction decreasing. Thus the substitution of Cr is clearly detrimental to the superconductivity in this system, either due to the substitution carrying excess oxygen into the system, or due to ensuing structural distortions, or both. Post-annealing in a reducing $Ar–H_2$ flow was attempted with a view to improve the superconducting properties, but to no effect. Such treatment is known to be useful in some of the thallium cuprates (23).

CONCLUSION

Cr seems to preferentially dope the Cu^I site in the ''0201–0212'' phases. If the Cr is actually present as CrO_4^{2-}, as suggested by the lattice images and the FTIR spectrum, the substitution could be compared with the replacement of Cu^I by CO_3^{2-} in the ''123'' cuprates (4). The present work adds to evidence for the rich structural chemistry possible with the superconducting cuprates. Particularly interesting is the substitution at the level of Cu^IO chains which exist in these and in the ''123'' structures, and are comparable, structurally, to the OHgO rods present in some of the superconducting mercury cuprates. Such substitution does not seem to destory superconductivity in these phases, further supporting the existence of Cr as the relatively inert (in terms of magnetism) Cr^{VI} in these systems.

ACKNOWLEDGMENTS

This work was supported by the European Community Grant CI1*-CT94-0107. We thank Dr. M. Daturi for help in acquiring the FTIR spectra.

REFERENCES

1. R. J. Cava, B. Batlogg, J. J. Krajewski, L. W. Rupp, L. F. Schneemeyer, T. Siegrist, R. B. van Dover, P. March, W. F. Peck, Jr., P. K. Gallagher, S. H. Glarum, J. H. Marshall, R. C. Farrow, J. V. Waszczak, R. Hull, and P. Trevor, *Nature* **336,** 211 (1988).
2. Y. Miyazaki, H. Yamane, N. Ohnishi, T. Kajitani, K. Hiraga, Y. Morii, S. Funahashi, and T. Hirai, *Physica C* **198,** 7 (1992); B. Raveau, M. Huve, A. Maignan, M. Hervieu, C. Michel, B. Domenges, and C. Martin, *Physica C* **209,** 163 (1993) and Eyelatt, January 1993.
3. Y. Miyazaki, H. Yamane, T. Kajitani, N. Kobayashi, K. Hiraga, Y. Morii, S. Funahashi, and T. Hirai, *Physica C* **230,** 89 (1994).
4. B. Domenges, M. Hervieu, and B. Raveau, *J. Phys. I* **207,** 65 (1993).
5. G. Roth, P. Adelman, G. Heger, and R. Knitter, *Physica C* **1,** 721 (1991).
6. T. G. N. Babu, D. J. Fish, and C. Greaves, *J. Mater. Chem.* **1,** 677 (1991).
7. K. Toriumi and Y. Saito, *Acta Crystallogr.* **34,** 3149 (1978).
8. T. G. N. Babu and C. Greaves, *Physica C* **207,** 44 (1993).
9. A. Ono, *Jpn. J. Appl. Phys.* **34,** L1528 (1995).
10. A. Maignan, D. Pelloquin, S. Malo, C. Michel, M. Hervieu, and B. Raveau, *Physica C* **243,** 233 (1995).
11. D. Pelloquin, A. Maignan, S. Malo, M. Hervieu, C. Michel, and B. Raveau, *J. Mater. Chem.* **5,** 701 (1995).
12. J. Shimoyama, S. Hahakura, K. Kitazawa, K. Yamafuji, and K. Kishio, *Physica C* **224,** 1 (1994).
13. S. Hahakura, J. Shimoyama, O. Shiino, T. Hasegawa, K. Kitazawa, and K. Kishio, *Physica C* **235,** 915 (1994).
14. O. Chmaissen, D. N. Argyriou, D. G. Hinks, J. D. Jorgensen, B. G.

Storey, H. Zhang, L. D. Marks, Y. Y. Wang, V. P. Dravid, and B. Dabrowski, *Phy. Rev. B* **235,** 15636 (1995).
15. C. Martin, F. Letouzé, A. Maignan, R. Seshadri, C. Michel, M. Hervieu, and B. Raveau, *Chem. Mater.* **8,** 865 (1995).
16. C. Michel, F. Letouzé, C. Martin, M. Hervieu, and B. Raveau, *Physica C* **262,** 159 (1996).
17. B. Raveau, C. Michel, and M. Hervieu, *C.R. Acad. Sci. Paris Ser. IIB* **322,** 609 (1996).
18. J. F. Bérar and P. Garnier, *in* ''Accuracy in Powder Diffraction,'' Proc. II Intl. Conf., Gaithersburg, 1992; *NIST Special Publ.* **846,** 212 (1992).
19. E. A. Hewat, J. J. Capponi, R. J. Cava, C. Chaillout, M. Marezio, and J. L. Tholence, *Physica C* **157,** 509 (1989).
20. H. W. Zandbergen, K. Kadowacki, M. J. V. Menken, A. A. Menowsky, G. van Tendeloo, and S. Amelinckx, *Physica C* **158,** 155 (1989).
21. T. Mochiku and K. Kadowacki, *J. Phys. Soc. Jpn.* **61,** 881 (1992).
22. J. Gopalakrishnan, *in* ''The Chemistry of High-Temperature Superconductors'' (C. N. R. Rao, Ed.), pp. 156–185. World Scientific, Singapore, 1991.
23. C. Martin, A. Maignan, J. Provost, C. Michel, M. Hervieu, R. Tournier, and R. Raveau, *Physica C* **168,** 8 (1990).